IEEE Access
Multidisciplinary | Rapid Review | Open Access Journal

Received November 25, 2018, accepted December 18, 2018, date of publication December 21, 2018,
date of current version January 23, 2019.

Digital Object Identifier 10.1109/ACCESS.2018.2889044

Low-Order Space Harmonic Modeling of Asymmetrical Six-Phase Induction Machines

AYMAN S. ABDEL-KHALIK[1], (Senior Member, IEEE), RAGI A. HAMDY[1], (Member, IEEE), AHMED M. MASSOUD[2], (Senior Member, IEEE), AND SHEHAB AHMED[3], (Senior Member, IEEE)

[1]Department of Electrical Engineering, Alexandria University, Alexandria 21544, Egypt
[2]Department of Electrical Engineering, Qatar University, Doha 2713, Qatar
[3]CEMSE Division, King Abdullah University of Science and Technology, Thuwal 23955, Saudi Arabia

Corresponding author: Ahmed M. Massoud (ahmed.massoud@qu.edu.qa)

ABSTRACT Multiphase machines are commonly analyzed using vector space decomposition modeling technique, where the original phase variables are decomposed into multiple orthogonal subspaces. The machine torque production and, therefore, its dynamic response are mainly decided from the α–β fundamental subspace. In the available literature, other non-fundamental subspaces are commonly regarded as the non-flux/torque producing subspaces while mainly contributing to the extra winding joule losses. Although the primitive harmonic-free models are usually assumed for these secondary subspaces in the asymmetrical six-phase induction machines, a clear evidence to include or discard the effect of the low-order space harmonics of the air gap flux distribution under different neutral configurations has not been established so far. To this end, this paper investigates the effect of the induced air gap harmonics mapped to the x-y and zero subspaces on the dynamic modeling and, hence, the dynamic response of an asymmetrical six-phase induction machine. An improved space harmonic model is, then, proposed to better explore/simulate their effect under both healthy as well as fault conditions. The proposed model is experimentally validated using a 1.5-kW prototype induction machine.

INDEX TERMS Asymmetrical six-phase, induction machine modeling, low-order space harmonics, scalar control, fault-tolerant, open phase, neutral configuration.

Nomenclature

i	Current
v	Voltage
λ	Flux linkage
R	Winding resistance
L	Self or magnetizing inductances
l	Leakage inductance
p	Number of pole pairs
T_d	Developed torque
n	number of stator phases
m_r	number of rotor bars
N_{ph}	number of turns per stator phase
$K_{w(h)}$	stator winding factor for a harmonic order$h$
$K_{skew(h)}$	cage rotor skew factor for a harmonic order$h$
	Subscripts
h	Harmonic order
α, β	Fundamental subspace components
x, y	Secondary subspace components
0_+, 0_-	Zero sequence components
s	Stator
r	Rotor
m	Magnetizing

I. INTRODUCTION

The multiphase machines have recently proved to prevail in high-power adjustable speed drives and multi-megawatt wind energy conversion systems that entail the operation under high performance and rigorous reliability standards alike [1]-[5]. For these applications, the superiority of multiphase drive systems over traditional three-phase alternatives cannot be overlooked. Thence, the research community has devoted a prodigious effort to shed light on the myriad privileges of this technology in different applications [1]. Undoubtedly, the dual three-phase machines are one of the most popular practical options in different industry sectors, owing to the possibility to employ the well-established

three-phase technology, ensuring that the required hardware modifications shall be in an acceptable tight window. The literature has demonstrated that a dual three-phase machine with a spatial phase shift of 30^0 between both three-phase sets, which is commonly recognized as asymmetrical six-phase (A6P) machines, leads to an improved flux distribution and, therefore, a higher torque quality [6]. The two three-phase winding sets can either be connected with isolated (2N) or connected (1N) neutral configurations, as shown in Fig. 1.

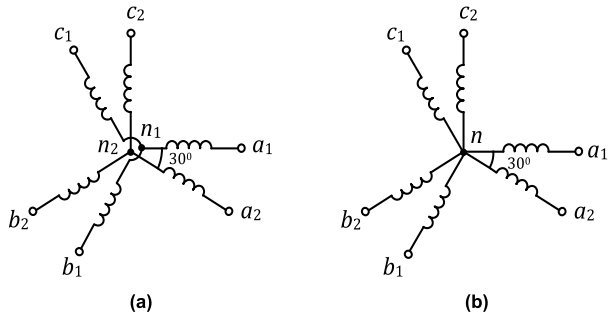

FIGURE 1. Possible neutral configurations for asymmetrical six-phase stator winding. (a) Isolated (2N) arrangement. (b) Connected (1N) arrangement.

Generally, mathematical modeling always pops up at the top of the research topics' list when investigating any practical system. The multiphase machine modeling has, therefore, met considerable attention among the research community since early stages and hitherto [7]-[16]. It is quite fair to acknowledge that the so-called vector space decomposition (VSD) modeling approach [6] is the most employed technique in utmost recent literature, where the n-phase machine variables are decomposed into a single $\alpha - \beta$ torque producing subspace and multiple orthogonal secondary subspaces. A widely employed assumption is to regard these secondary x-y subspaces as non-flux/torque producing subspaces [6]. This assumption originates from the fact that the higher the number of phases is, the more sinusoidal flux distribution will then be, even for concentrated single layer windings. However, this assumption can sufficiently be valid under only healthy condition, where the effect of all secondary subspaces is ideally nullified.

The up-to-date literature has demonstrated a thorough investigation of time-harmonic mapping among different subspaces of multiphase windings [17], [18]. These studies have been the baseline on which multi-frequency current control was then proposed to compensate for these parasitic harmonic current components [19]-[21]. On the other hand, the interest to investigate/model the effect of different space harmonics in multiphase winding has not met the same attention so far. This indifference was logically driven by the well-established assumptions made in the literature that the harmonic flux components produced by the secondary subspaces can be ignored. However, regardless the current waveform is being sinusoidal or distorted, space harmonic mitigation can only be carried out through innovative winding layouts rather than current control. The harmonic current compensation will actually help prevent the distortion of the developed torque profile with more undesirable ripple torque components. Thus, a clear evidence to discard the effect of these low-order space harmonics on the machine dynamics has not evidently been yet confirmed.

Recent studies have, however, shown a notable effect of these low-order harmonics especially under fault conditions [22]-[24]. The study given in [22] has proven that the induced third harmonic air gap flux component in an A6P IM under zero-sequence current excitation affects the accuracy of the input impedance estimation of this subspace. Being a stationary flux component in nature, this third harmonic component will expectedly introduce a subsynchronous speed point in the torque-speed curve under fault conditions at one-third the machine rated synchronous speed. Recent studies also have shown a notable third harmonic induction under fault conditions for the five-phase induction machine case [23], which likely affects the machine dynamic performance [24], [25]. The first attempt to include the effect of third harmonic flux component in the mathematical model of a symmetrical six-phase induction machine in order to better estimate the steady-state phase current waveforms has been introduced in [26], [27]. To the best of the authors' knowledge, no further attention has been paid to investigate the effect of low space harmonics on the mathematical model of induction machines with other six-phase winding layouts under the two possible neutral arrangements.

This paper first introduces the effect of different stator excitations of the air gap space harmonics of an A6P stator. An improved low-order space harmonic model for the three subspaces is, then, proposed in Section III. The dominant low-order harmonics, namely 3^{rd}, 5^{th}, and 7^{th} order air gap space harmonics, commonly mapped to the x-y and zero subspaces, are included in this proposed model to better estimate the machine dynamic performance under healthy as well as fault conditions. Experimental validation to the proposed model is given in Section IV using a 1.5kW prototype induction machine. Finally, the main conclusions behind this study are reported in Section V.

II. DOMINANT LOW-ORDER SPACE HARMONICS IN DIFFERENT SUBSPACES OF ASYMMETRICAL SIX-PHASE WINDINGS

It is a matter of fact that the air gap flux distribution of the primary subspace of any multiphase winding contains numerous undesirable space harmonic components among them are the phase belt harmonics of order $h = 2qj \pm 1$ [28], where j is any positive integer, $q = 180^0/\delta$, and δ is the winding phase belt angle.

From a practical perspective, an A6P winding can be constructed from a traditional three-phase stator by simply splitting the winding phase belt into two halves, yielding $\delta = 30^0$. Based on the space harmonic order, different harmonics are, therefore, mapped to specific subspaces. The $\alpha - \beta$ subspace holds the $6j \pm 1$ harmonics, where $j = \{0, 2, 4, 6, \ldots\}$,

the $6i \pm 1$ harmonics are mapped to the x-y subspace, where $i = \{1, 3, 5, \ldots\}$, while the 0_+0_- subspace is concerned with the triplen harmonics (3^{rd}, 9^{th}, 15^{th}, ...).

The lowest order harmonics will, thus, be the 11^{th} and 13^{th} under $\alpha - \beta$ current excitation. In case of x-y secondary current excitation, the 5^{th} and 7^{th} low-order harmonics represent the dominant harmonics of this subspace. The magnitude of these space harmonic components will largely depend on the stator winding layout. For a sinusoidally distributed winding, these harmonic components shall theoretically be eliminated. For the zero-sequence subspace, the air gap flux distribution experiences a stationary third harmonic component with a magnitude depending on the employed winding layout as well. Practically, a 5/6 double layer winding is commonly employed in A6P induction machines [29] to minimize the stator leakage inductance [30]. However, it has been demonstrated in [22] using a 5/6 double layer A6P winding that the harmonic spectrum of the zero subspace explores non-negligible third harmonic component. Based on the notable magnetomotive force (MMF) component of this third harmonic component, an improved equivalent circuit has been proposed to help identifying the machine different leakage inductance components in higher accuracy.

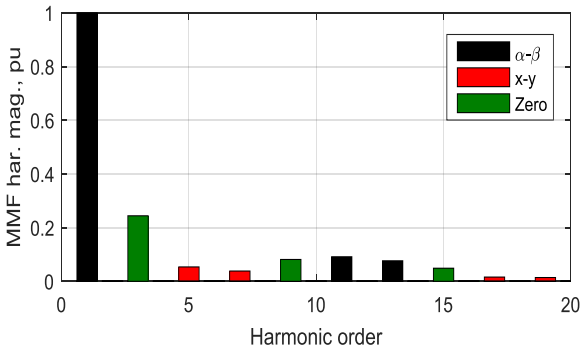

FIGURE 2. MMF spectra under different sequence excitations.

To recall this phenomenon, Fig. 2 depicts the different MMF spectra under the three possible excitations of an A6P stator using a 12-slot/pole-pair stator and a winding pitch of 5/6. Under x-y subspace excitation, the 5^{th} and 7^{th} harmonics have 5.4% and 4% magnitudes relative to the fundamental component. While under zero sequence excitation, the 3^{rd} harmonic component has a relative magnitude of 24.4%. Hence, neglecting these harmonic components may cause a notable deviation in the predicted machine performance, especially under transient operation, in comparison to the obtained results based on the widely used harmonic-free model.

III. PROPOSED VSD MODEL

The dynamic modeling for multiphase machine is mostly based on VSD modeling. The n-phase Clarke's transformation is used to decompose the phase quantities (i.e., current, voltage, and flux linkage) into orthogonal stationary subspaces. For an A6P machine, the six-phase quantities are

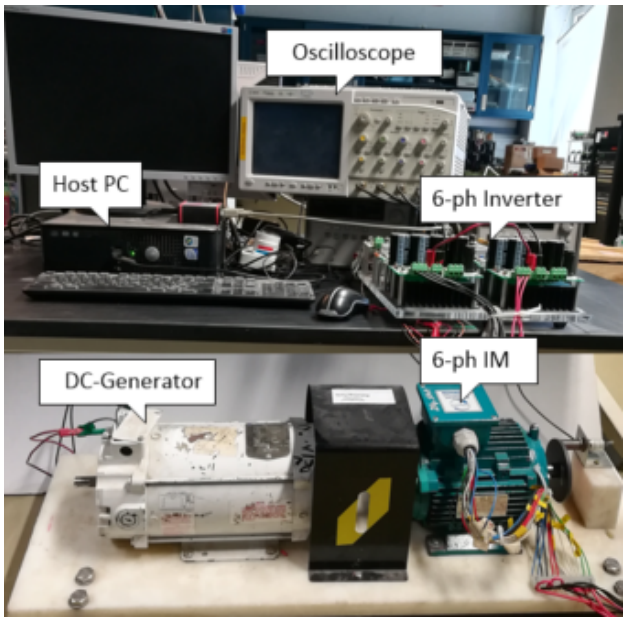

FIGURE 3. Experimental Setup.

decomposed to three orthogonal planes, namely the $\alpha - \beta$ subspace, the x-y subspace, and the 0_+0_- subspace. The $\alpha - \beta$ subspace is the main torque producing subspace. For a balanced healthy winding, the other two subspaces will be nullified; their effect, therefore, appears mainly under unbalanced conditions. The VSD matrix employed for an A6P stator is defined as,

$$[T] = \frac{1}{\sqrt{3}} \times \begin{bmatrix} 1 & -0.5 & -0.5 & 0.866 & -0.866 & 0 \\ 0 & 0.866 & -0.866 & 0.5 & 0.5 & -1 \\ 1 & -0.5 & -0.5 & -0.866 & 0.866 & 0 \\ 0 & -0.866 & 0.866 & 0.5 & 0.5 & -1 \\ 0.5 & 0.5 & 0.5 & 0 & 0 & 0 \\ 0 & 0 & 0 & 0.5 & 0.5 & 0.5 \end{bmatrix} \quad (1)$$

It is recognized that including more harmonics in the machine model will certainly improve the modeling accuracy at the cost of model complexity and computational burden. The best compromise is to consider only the dominant low-order phase belt space harmonics in each subspace, which will likely affect the average torque as well as torque ripple production. Higher order harmonics will, therefore, be neglected in this study. The general assumptions that will also be made are as follows:

1) The magnetic circuit is assumed linear, and the effect of hysteresis, as well as eddy current losses, will be discarded [31].
2) The effect of slot harmonics is neglected.
3) All sources of winding asymmetries will be ignored.

Based on these assumptions, the $\alpha - \beta$ subspace will be responsible for the fundamental torque producing flux

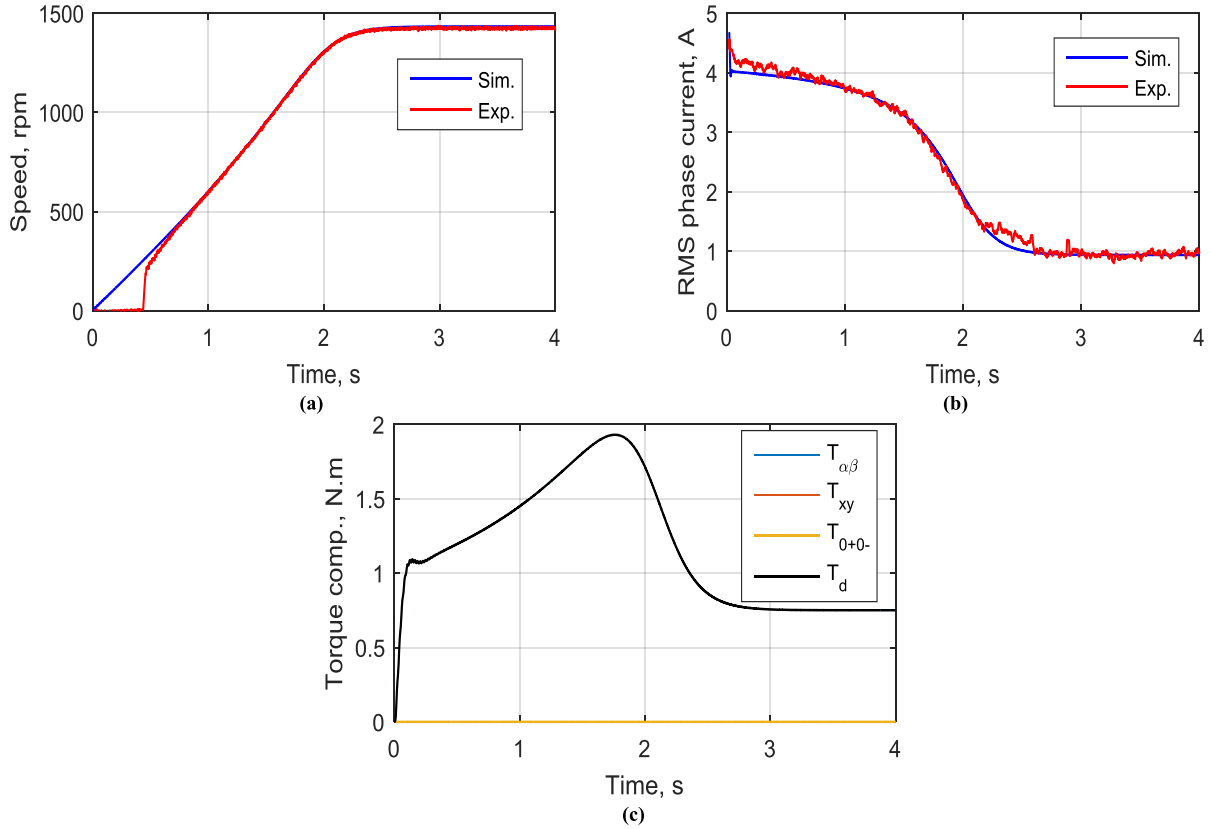

FIGURE 4. Open-loop free-running mode results for the healthy case. (a) Speed. (b) RMS phase current. (c) Average torque components.

component, the x-y subspace will represent the effect of the 5^{th} and 7^{th} space harmonics, and the 0_+0_- subspace will account for the effect of the air gap third harmonic flux component.

A. MACHINE VOLTAGE EQUATIONS

The proposed machine model will comprise three decoupled subspaces. Since the fundamental torque producing component is mapped to the fundamental $\alpha - \beta$ subspace, the conventional voltage equations of a traditional three-phase system will hold.

$$v_{\alpha s} = R_s i_{\alpha s} + p\lambda_{\alpha s} \tag{2}$$
$$v_{\beta s} = R_s i_{\beta s} + p\lambda_{\beta s} \tag{3}$$
$$0 = R_r i_{\alpha r} + p\lambda_{\alpha r} + \omega_r \lambda_{\beta r} \tag{4}$$
$$0 = R_r i_{\beta r} + p\lambda_{\beta r} - \omega_r \lambda_{\alpha r} \tag{5}$$

The flux linkage equations for this subspace are given by

$$\lambda_{\alpha s} = (l_{s1} + L_{m1})\, i_{\alpha s} + L_{m1} i_{\alpha r} \tag{6}$$
$$\lambda_{\beta s} = (l_{s1} + L_{m1})\, i_{\beta s} + L_{m1} i_{\beta r} \tag{7}$$
$$\lambda_{\alpha r} = L_{m1} i_{\alpha s} + (l_{r1} + L_{m1})\, i_{\alpha r} \tag{8}$$
$$\lambda_{\beta r} = L_{m1} i_{\beta s} + (l_{r1} + L_{m1})\, i_{\beta r} \tag{9}$$

For the x-y subspace, the same x-y stator current components will give rise to 5^{th} and 7^{th} order harmonics in the air gap flux. Hence, the suggested voltage equations for this subspace, which is inspired from the traditional three-phase case [32] to represent the effect of low-order space harmonics, will be as follows:

$$v_{xs} = R_s i_{xs} + p\lambda_{xs} \tag{10}$$
$$v_{ys} = R_s i_{ys} + p\lambda_{ys} \tag{11}$$
$$0 = R_{r5} i_{xr5} + p\lambda_{xr5} + 5\omega_r \lambda_{yr5} \tag{12}$$
$$0 = R_{r5} i_{yr5} + p\lambda_{yr5} - 5\omega_r \lambda_{xr5} \tag{13}$$
$$0 = R_{r7} i_{xr7} + p\lambda_{xr7} - 7\omega_r \lambda_{yr7} \tag{14}$$
$$0 = R_{r7} i_{yr7} + p\lambda_{yr7} + 7\omega_r \lambda_{xr7} \tag{15}$$

In this representation, the stator circuit is represented by two voltage equations, while the rotor circuit is modeled using four equations (two for each space harmonic). The corresponding flux linkage equation for this subspace will be as follows;

$$\lambda_{xs} = \left(l_{sxy} + L_{m5} + L_{m7}\right) i_{xs} + L_{m5} i_{xr5} + L_{m7} i_{xr7} \tag{16}$$
$$\lambda_{ys} = \left(l_{sxy} + L_{m5} + L_{m7}\right) i_{ys} + L_{m5} i_{yr5} + L_{m7} i_{yr7} \tag{17}$$
$$\lambda_{xr5} = L_{m5} i_{xs} + (l_{r5} + L_{m5})\, i_{xr5} \tag{18}$$
$$\lambda_{yr5} = L_{m5} i_{ys} + (l_{r5} + L_{m5})\, i_{yr5} \tag{19}$$
$$\lambda_{xr7} = L_{m7} i_{xs} + (l_{r7} + L_{m7})\, i_{xr7} \tag{20}$$
$$\lambda_{yr7} = L_{m7} i_{ys} + (l_{r7} + L_{m7})\, i_{yr7} \tag{21}$$

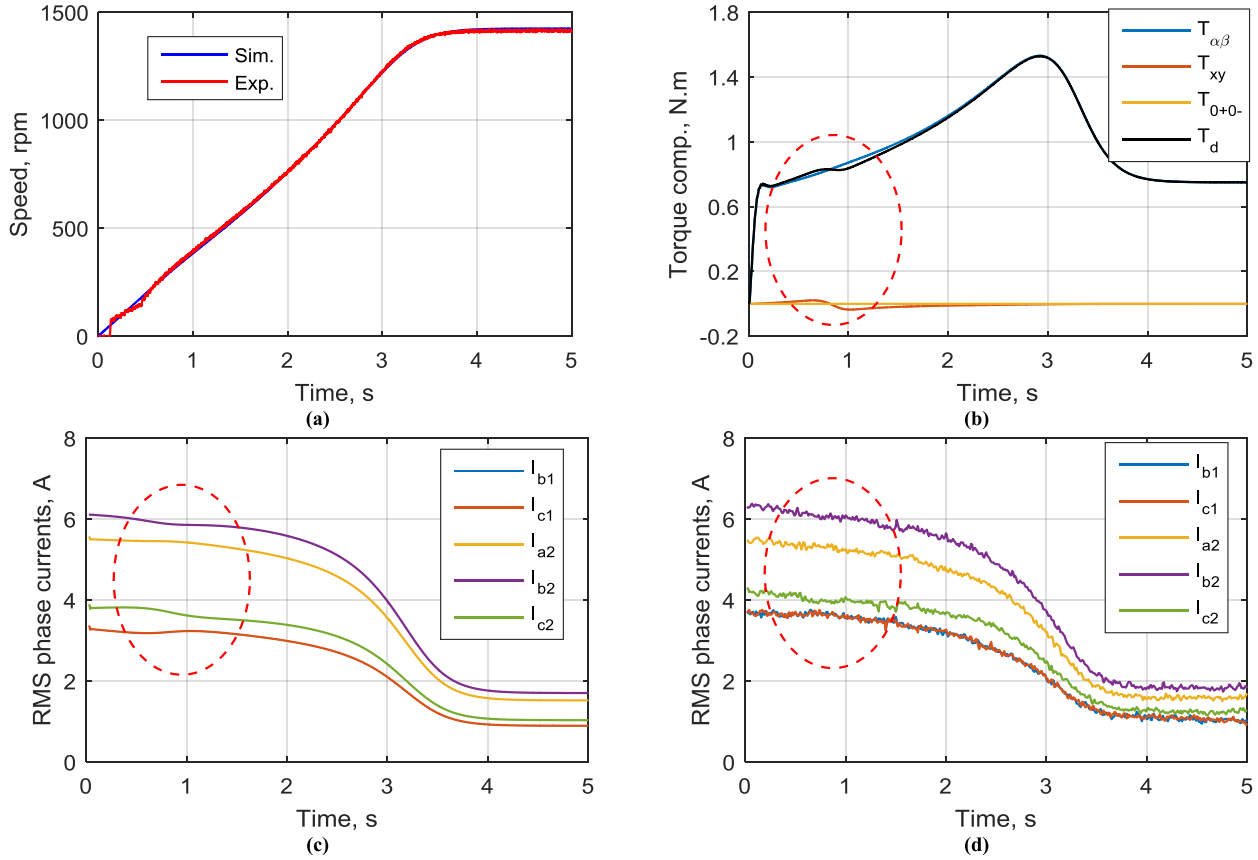

FIGURE 5. Open-loop free-running mode results for phase a_1 case and isolated neutrals (2N). (a) Speed. (b) Average torque components. (c) Simulated RMS phase currents. (d) Experimental RMS phase currents.

Clearly, from the voltage equations of this subspace, there will be two subsynchronous speed points at one-fifth and one-seventh the fundamental synchronous speed. The speed voltage terms that correspond to the 5th and 7th harmonics have also different signs to account for the opposite directions of these two space harmonics.

When the stator is fed from a zero-sequence excitation, the main dominant air gap harmonic will be the third. Similarly, the proposed voltage equations for this subspace will be as follows,

$$v_{0s+} = R_s i_{0s+} + p\lambda_{0s+} \tag{22}$$
$$v_{0s-} = R_s i_{0s-} + p\lambda_{0s-} \tag{23}$$
$$0 = R_{r3} i_{0r+} + p\lambda_{0r+} + 3\omega_r \lambda_{0r-} \tag{24}$$
$$0 = R_{r3} i_{0r-} + p\lambda_{0r-} - 3\omega_r \lambda_{0r+} \tag{25}$$

The flux linkage equations will be then

$$\lambda_{0s+} = (l_{s3} + L_{m3})\, i_{0s+} + L_{m3} i_{0r+} \tag{26}$$
$$\lambda_{0s-} = (l_{s3} + L_{m3})\, i_{0s-} + L_{m3} i_{0r-} \tag{27}$$
$$\lambda_{0r+} = L_{m3} i_{0s+} + (l_{r3} + L_{m3})\, i_{0r+} \tag{28}$$
$$\lambda_{0r-} = L_{m3} i_{0s-} + (l_{r3} + L_{m3})\, i_{0r-} \tag{29}$$

The torque components corresponding to the three subspaces are calculated from;

$$T_d^{\alpha\beta} = pL_{m1}\left(i_{\beta s} i_{\alpha r} - i_{\alpha s} i_{\beta r}\right) \tag{30}$$

$$T_d^{xy} = 5pL_{m5}\left(i_{ys} i_{xr5} - i_{xs} i_{yr5}\right) + 7pL_{m7}\left(i_{ys} i_{xr7} - i_{xs} i_{yr7}\right) \tag{31}$$

$$T_d^{0+0-} = 3pL_{m3}\left(i_{0s-} i_{0r+} - i_{0s+} i_{0r-}\right) \tag{32}$$

The total torque is then given by

$$T_d = T_d^{\alpha\beta} + T_d^{xy} + T_d^{0+0-} \tag{33}$$

It is worth mentioning that the torque components T_d^{xy} and T_d^{0+0-} are usually neglected in all available literature. Including the effect of these components in the machine dynamic performance estimation will, therefore, represent a main contribution of this proposed model.

B. PARAMETERS OF NON-FUNDAMENTAL SUBSPACES

An important step to properly model different subspaces is to identify the magnetizing as well as the rotor circuit parameters of all subspaces. The study introduced in [22] proposed an improved equivalent circuit to the zero subspace, which was also shown effective to better identify the machine different leakage inductance components. It has been also proved in [23] that the ratio between the magnetizing coupling inductance corresponding to any space harmonic of order, h, and the fundamental magnetizing inductance of a multiphase winding is inversely proportional to the harmonic order squared. This fact introduces a practical limitation to properly identify the rotor circuit parameters of the

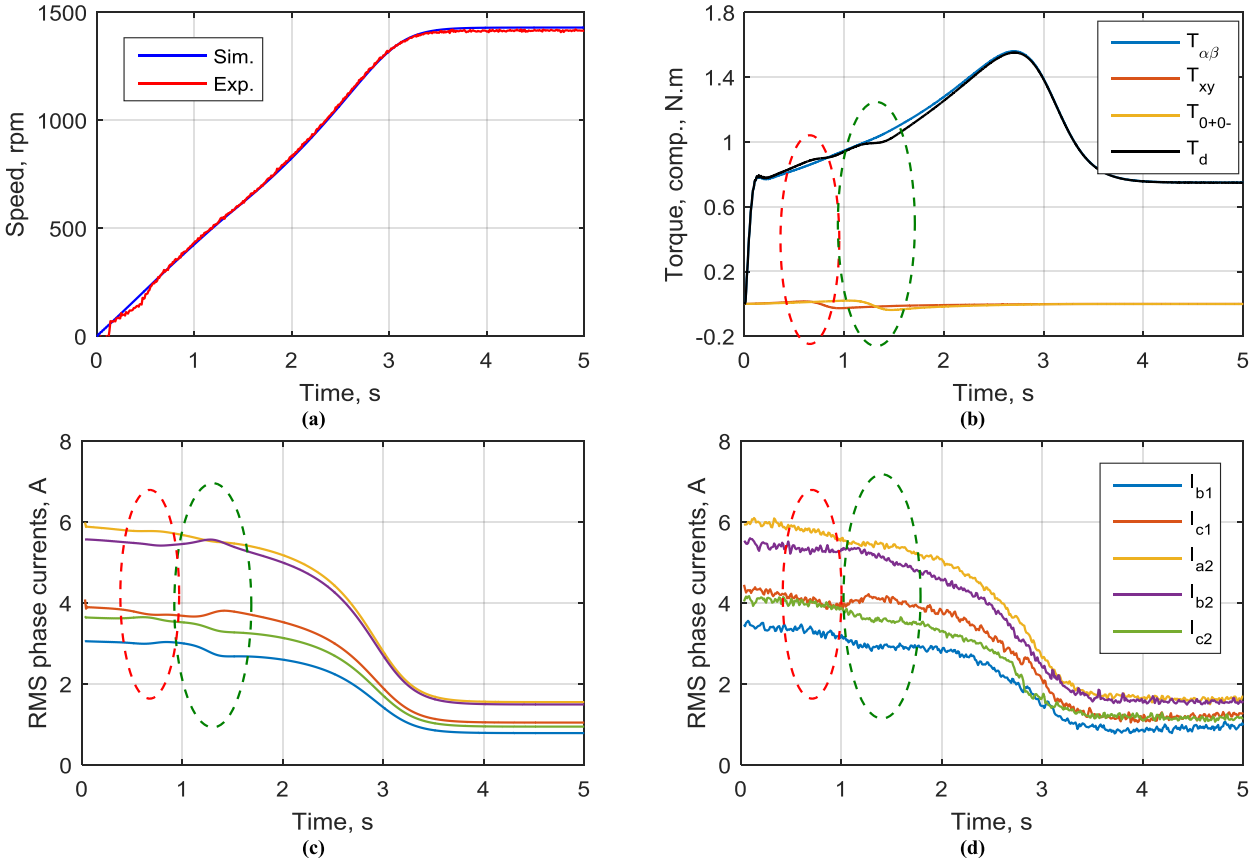

FIGURE 6. Open-loop free-running mode results for phase a_1 case and connected neutrals (1N). (a) Speed. (b) Average torque components. (c) Simulated RMS phase currents. (d) Experimental RMS phase currents.

non-fundamental subspaces based on experimental measurements. In [22] and [33], a simple technique is employed to roughly estimate these parameters from those of the fundamental circuit. This is carried out by first representing the rotor circuit parameters of different subspaces as functions of the cage circuit parameters using:

$$R_{rh} = \frac{4n}{m_r}\left(\frac{N_{ph}K_{w(h)}}{K_{skew(h)}}\right)^2 r_{be} \tag{34}$$

$$l_{rh} = \frac{4n}{m_r}\left(\frac{N_{ph}K_{w(h)}}{K_{skew(h)}}\right)^2 l_{be} \tag{35}$$

where r_{be} and l_{be} are the equivalent bar and end ring segment resistance and inductance, respectively.

Based on (34) and (35), the rotor circuit parameters referred to the stator side can be represented as functions of those of the fundamental subspace as,

$$R_{rh} = C_{h1}R_{r1} \text{and } l_{rh} = C_{h1}l_{r1} \tag{36}$$

where C_{h1} is defined as

$$C_{h1} = \left(\frac{K_{w(h)}}{K_{w(1)}} \cdot \frac{K_{skew(1)}}{K_{skew(h)}}\right)^2 \tag{37}$$

The magnetizing inductance of each space harmonic can also be approximated using the following relation [23],

$$L_{mh} = \left(\frac{K_{w(h)}}{hK_{w(1)}}\right)^2 L_{m1} \tag{38}$$

The techniques employed in [22] or [34] can simply be used to decide the parameters of the $\alpha - \beta$ as well as the zero subspaces. Then, the rotor parameters of the remaining x-y subspace are then calculated based on (36), while the magnetizing inductances of different space harmonics are estimated using (38).

IV. MODEL VERIFICATION

A. EXPERIMENTAL PROTOTYPE SYSTEM

The proposed model is investigated using a 1.5kW prototype induction machine, which has been constructed by rewinding a standard 4-pole, 380V, 50Hz, three-phase IM while preserving same rated current. The new winding maintains the same total number of conductors per slot and the same conductor cross-sectional area. The 24-slot stator is equipped with a double layer winding with 5/6 winding pitch. The new machine rated values after rewinding process are given in Table 1. The machine is fed from two three-phase inverters connected to the same dc-link and controlled using traditional sinusoidal pulse width modulation (PWM) at a 5kHz

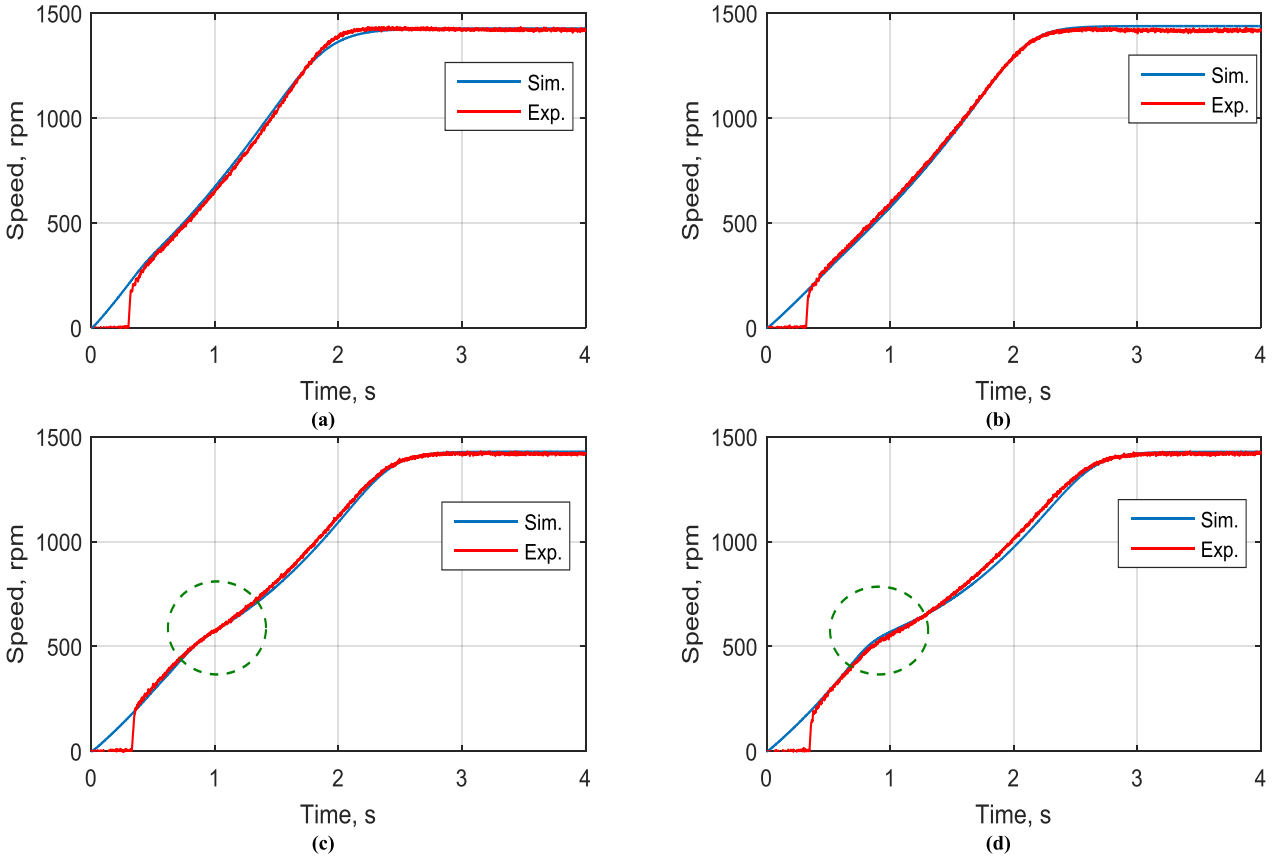

FIGURE 7. The machine speed profile under optimal current control and phase a1 open. (a) MT2N. (b) ML2N. (c) MT1N. (d) ML1N.

TABLE 1. Prototype IM specifications.

Rated phase voltage (V)	110	Rated frequency (Hz)	50
Rated Power (kW)	1.5	Rated speed (rpm)	1420
Rated phase current (A)	3.4	Pole number	4

switching frequency. The whole experimental setup is shown in Fig. 3. The technique given in [22] is used to estimate the machine parameters and are given in Table 2.

TABLE 2. Estimated machine parameters of different subspaces.

Subspace /Harmonic		r_{sk} (Ω)	l_{sk} (mH)	r_{rk} (Ω)	l_{rk} (mH)	L_{mk} (mH)
α-β	$k=1$	2	11.4	1.95	12.9	161
0_+0_-	$k=3$	2	7.8	0.995	6.58	14.4
x-y	$k=5$	2	1.46	0.195	1.29	0.934
	$k=7$	2	1.46	0.39	2.58	0.242

It is worth noting that the effect of low-order space harmonics is mainly showing up under transient conditions and fault conditions. The best way to explore this effect is to simulate the machine starting up condition under open-loop speed control with one phase disconnected. For this case, the torque-speed curve will exhibit clear subsynchronous speed points as a consequence of the presence of the low-order space harmonics. This will mainly affect the motor acceleration and speed starting up profiles due to the corresponding induced parasitic torque components. Under closed-loop speed control, these problems can easily be compensated for [35]. Hence, it will not be recruited in this validation study. It is also fair to say that the harmonic free model can properly simulate the machine under steady-state conditions since the effect of these secondary subspaces will be merely neglected [34]. Therefore, the simulation, as well as the experimental validation, will only be given for the motor starting period where the target phenomenon will be evident.

In the following subsections, the simulation results obtained based on the proposed model are validated using experimental measurements under both open-loop free-running mode and optimal current control based on scalar V/f control given in [36].

B. FREE-RUNNING MODE

In this case, the inverter reference fundamental frequency is set to 50Hz, while the applied voltage is set to a reduced stator voltage (50V) to avoid high inrush starting currents, which saturates the current measuring boards. The friction torque will dominate in this case. For the sake of comparison, the machine is simulated under the same conditions. Interestingly, the voltage magnitude reduction will only increase the starting time but has no notable effect

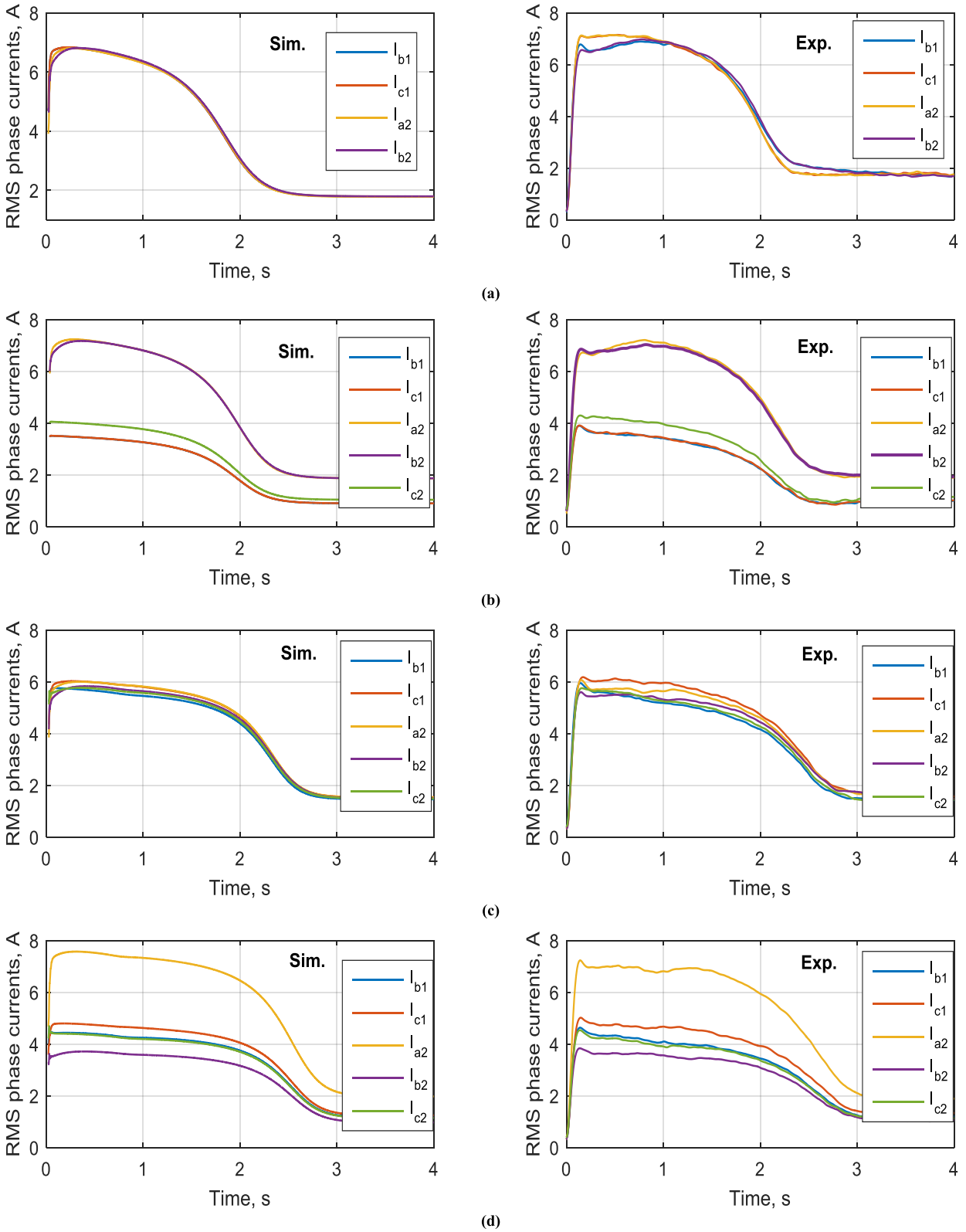

FIGURE 8. The simulation and experimental results of machine RMS phase current profiles under optimal current control and phase a1 open. (a) MT2N. (b) ML2N. (c) MT1N. (d) ML1N.

on the speed profile if core saturation is to be ignored, which is the assumed case for this study. The increase in starting time due to voltage reduction will also be valuable to better depict the machine transient due to these small space harmonic components by prolonging this transient period.

Figs. 4(a) and (b) compare the simulation and experimental profiles for both speed and RMS phase current, respectively, under healthy conditions (shown here as a benchmark case). It may be fair to assume that the simulation results coincide with a satisfactory degree to the experimental results, which validates the proposed model under healthy conditions. The simulated average torque components during starting are shown in Fig. 4(c). Clearly, all torque components otherwise fundamental ($\alpha - \beta$ subspace) will add to zero under this case.

Figs. 5 and 6 show the same comparison for the fault case with phase a_1 disconnected and under isolated and connected neutrals arrangements, respectively. As a matter of fact, phase loss will reduce the maximum achievable torque due to the reduction in fundamental voltage components [34]. Therefore, the machine takes a longer time than the healthy case to reach its final steady-state speed. Under open-loop current control, a notable magnitude diversion between different phases is evident, which also gives rise to secondary torque components, as shown in Figs. 5(b) and 6(b).

Under the 2N arrangement, the zero-sequence component is blocked; and hence, the effect of this subspace is nullified. The total average torque, shown in Fig. 5(b), experiences a small dip in the torque profile during starting due to the effect of the 5^{th} harmonic of the x-y subspace, this effect is highlighted by the red dashed ellipse around a speed of 300 rpm (one-fifth rated synchronous speed). On the other hand, and under the 1N arrangement, the effect of the zero-sequence current component comes into play by introducing another torque dip, but with a larger magnitude, in the accelerating torque profile given in Fig. 6(b) around a speed of 500 rpm (one-third rated synchronous speed), which represents the effect of the 3^{rd} harmonic component. This is highlighted by the green shaded ellipse in the same figure. Aligned with the conclusion based on Fig. 2, the effect of the third harmonic due to zero sequence current components sounds more effective than the 5^{th} and 7^{th} harmonic. Clearly, the obtained simulation results agree, with a large extent, with the experimental results, which supports the fidelity of the proposed model to better explore the effect of these space harmonics under fault conditions.

C. OPTIMAL CURRENT CONTROL

In this subsection, the simulation model is validated under open phase conditions, where the remaining healthy phases are optimally controlled to achieve either maximum torque per ampere (MT) operation or minimum stator copper loss (ML) operation [36]. The V/f-based controller given in [36] is employed in this study. The full controller structure is detailed in [36], where the reference voltage components of the fundamental $\alpha - \beta$ subspace are generated based on traditional V/f scalar control. It has been explained in [36] that based on the selected postfault scenario (MT or ML) and the neutral arrangement (2N or 1N), there are set of reference optimal currents that can be achieved by controlling the voltage components of the x-y and zero subspaces. The required voltage components of the non-fundamental subspaces are derived from the current error of the corresponding sequence current components using four proportional-resonant (PR) controllers.

The experimental results given based on this controller are compared with the simulations obtained based on the proposed mathematical model. The fundamental voltage magnitude is set to 50V at 50Hz frequency. The speed and RMS phase current profiles under both modes and with both neutral arrangements are given in Figs. 7 and 8, respectively. The good agreement obtained under open-loop operation is also obtained under optimal current control. This proves that the mathematical model along with the estimated machine parameters can properly simulate the effect of low-order space harmonic on the machine starting behavior.

Under the 2N arrangements (Figs. 7(a) and (b)), the effect of the fifth order harmonic can safely be ignored. On the other hand, the third order harmonic component, caused by the flow of the zero-sequence component with the winding configured with a single neutral point, yields a notable speed dip around one-third the rated synchronous speed as shown in Figs. 7(c) and (d). This represents a clear evidence to the notable presence of this space harmonic component and is also evident from the longer starting time obtained under this neutral arrangement. The effect of this component also sounds more effective under the ML rather than the MT scenario. Comparing the simulation and experimental results for the RMS phase currents shows very close agreement over the whole acceleration period, which obviously supports the validity of the proposed model.

V. CONCLUSION

This paper introduced an improved dynamic mathematical model for asymmetrical six-phase IMs based on the well-known VSD modeling approach, which incorporates the effect of the phase belt harmonics of the stator MMF. The proposed model was employed to simulate the machine under free-running open-loop control as well as optimal current control, and the obtained simulated results were experimentally verified. When compared with the widely employed harmonic-free model of an A6P IM, the proposed model was capable of exploring the subsynchronous speed points in the torque-speed curve due to the effect of the third and fifth order harmonics, which are typically mapped to the zero and x-y subspaces, respectively. The former harmonic only takes place under the single neutral arrangement, while the latter represents the dominant harmonic for the x-y subspace. The effect simply appears as multiple speed dips during the speed starting up under open phase conditions, with a negligible effect under steady-state operation. This, in turn, prolongs the machine starting time based on the adopted postfault scenario and/or the neutral arrangement. It is also fair to say that the third order space harmonic of the zero subspace sounds more effective than the fifth and seventh order harmonics of the x-y subspace. Based on the obtained results, the

harmonic-free model can still be preserved for the *x*-*y* subspace but cannot be adopted for the zero-sequence subspace. This conclusion resonates well with the obtained large amplitude of the third order space harmonic under zero-sequence excitation compared with those of the other space harmonics. Nevertheless, the effect of this third order harmonic component will only be limited to the transient periods. Therefore, closed-loop speed control can simply be used to compensate for this parasitic effect.

REFERENCES

[1] M. J. Duran, E. Levi, and F. Barrero, "Multiphase electric drives: Introduction," in *Encyclopedia of Electrical and Electronics Engineering*. Hoboken, NJ, USA: Wiley, 2017.

[2] X. Sun, L. Chen, H. Jiang, Z. Yang, J. Chen, and W. Zhang, "High-performance control for a bearingless permanent-magnet synchronous motor using neural network inverse scheme plus internal model controllers," *IEEE Trans. Ind. Electron.*, vol. 63, no. 6, pp. 3479–3488, Jun. 2016.

[3] X. Sun, Z. Shi, L. Chen, and Z. Yang, "Internal model control for a bearingless permanent magnet synchronous motor based on inverse system method," *IEEE Trans. Energy Convers.*, vol. 31, no. 4, pp. 1539–1548, Dec. 2016.

[4] X. Sun, L. Chen, Z. Yang, and H. Zhu, "Speed-sensorless vector control of a bearingless induction motor with artificial neural network inverse speed observer," *IEEE/ASME Trans. Mechatronics*, vol. 18, no. 4, pp. 1357–1366, Aug. 2013.

[5] X. Sun, B. Su, L. Chen, Z. Yang, X. Xu, and Z. Shi, "Precise control of a four degree-of-freedom permanent magnet biased active magnetic bearing system in a magnetically suspended direct-driven spindle using neural network inverse scheme," *Mech. Syst. Signal Process.*, vol. 88, pp. 36–48, May 2017.

[6] E. Levi, R. Bojoi, F. Profumo, H. A. Toliyat, and S. Williamson, "Multiphase induction motor drives—A technology status review," *IET Electr. Power Appl.*, vol. 1, no. 4, pp. 489–516, 2007.

[7] T. S. de Souza, R. R. Bastos, and B. J. C. Filho, "Modeling and control of a nine-phase induction machine with open phases," *IEEE Trans. Ind. Appl.*, vol. 54, no. 6, pp. 6576–6585, Nov./Dec. 2018.

[8] I. Zoric, M. Jones, and E. Levi, "Arbitrary power sharing among three-phase winding sets of multiphase machines," *IEEE Trans. Ind. Electron.*, vol. 65, no. 2, pp. 1128–1139, Feb. 2018.

[9] C. Gor, P. Gupta, V. Shah, and M. Lokhande, "Real time simulation of multiphase induction motor for electric vehicle using RT-lab," in *Proc. Conf. IECON*, Nov. 2017, pp. 6646–6651.

[10] M. Ayala *et al.*, "Modeling and analysis of dual three-phase self-excited induction generator for wind energy conversion systems," in *Proc. Conf. SPEC*, Dec. 2017, pp. 1–6.

[11] A. Pantea *et al.*, "Fault-tolerant control of a low-speed six-phase induction generator for wind turbines," *IEEE Trans. Ind. Appl.*, vol. 55, no. 1, pp. 426–436, Jan./Feb. 2019.

[12] M. A. Fnaiech, F. Betin, and G. A. Capolino, "A 5 × 5 model of the six phase squirrel cage induction machine (6PIM) in faulted condition," in *Proc. Conf. ISIE*, Jul. 2010, pp. 2129–2134.

[13] A. Pantea *et al.*, "Six-phase induction machine model for electrical fault simulation using the circuit-oriented method," *IEEE Trans. Ind. Electron.*, vol. 63, no. 1, pp. 494–503, Jan. 2016.

[14] S. Gradev, D. Findeisen, T.-L. Toennesen, and H.-G. Herzog, "A voltage-behind-reactance model of a dual-voltage six-phase induction machine," in *Proc. Conf. ICEM*, Sep. 2014, pp. 672–678.

[15] L. A. Pereira, C. C. Scharlau, L. F. A. Pereira, and J. F. Haffner, "General model of a five-phase induction machine allowing for harmonics in the air gap field," *IEEE Trans. Energy Convers.*, vol. 21, no. 4, pp. 891–899, Dec. 2006.

[16] A. S. Abdel-Khalik, S. Ahmed, A. A. Elserougi, and A. M. Massoud, "A voltage-behind-reactance model of five-phase induction machines considering the effect of magnetic saturation," *IEEE Trans. Energy Convers.*, vol. 28, no. 3, pp. 576–592, Sep. 2013.

[17] J. Malvar *et al.*, "Graphical diagram for subspace and sequence identification of time harmonics in symmetrical multiphase machines," *IEEE Trans. Ind. Electron.*, vol. 61, no. 1, pp. 29–42, Jan. 2014.

[18] A. G. Yepes, J. Malvar, A. Vidal, O. López, and J. Doval-Gandoy, "Current harmonics compensation based on multiresonant control in synchronous frames for symmetrical *n*-phase machines," *IEEE. Trans. Ind. Electron.*, vol. 62, no. 5, pp. 2708–2720, May 2015.

[19] L. Harnefors, A. G. Yepes, A. Vidal, and J. Doval-Gandoy, "Multifrequency current control with distortion-free saturation," *IEEE J. Emerg. Sel. Topics Power Electron.*, vol. 4, no. 1, pp. 37–43, Mar. 2016.

[20] A. G. Yepes, J. Doval-Gandoy, F. Baneira, D. Pérez-Estévez, and Ö. López, "Current harmonic compensation for *n*-phase machines with asymmetrical winding arrangement and different neutral configurations," *IEEE Trans. Ind. Appl.*, vol. 53, no. 6, pp. 5426–5439, Nov./Dec. 2017.

[21] A. G. Yepes, J. Doval-Gandoy, and H. A. Toliyat, "Multifrequency current control including distortion-free saturation and antiwindup with enhanced dynamics," *IEEE Trans. Power Electron.*, vol. 33, no. 9, pp. 7309–7313, Sep. 2018.

[22] H. S. Che, A. S. Abdel-Khalik, O. Dordevic, and E. Levi, "Parameter estimation of asymmetrical six-phase induction machines using modified standard tests," *IEEE Trans. Ind. Electron.*, vol. 64, no. 8, pp. 6075–6085, Aug. 2017.

[23] A. S. Abdel-Khalik, M. I. Daoud, S. Ahmed, A. A. Elserougi, and A. M. Massoud, "Parameter identification of five-phase induction machines with single layer windings," *IEEE Trans. Ind. Electron.*, vol. 61, no. 10, pp. 5139–5154, Oct. 2014.

[24] L. A. Pereira, L. F. A. Pereira, and S. Haffner, "Airgap induction of five-phase induction machines operating with one opened phase," in *Proc. Conf. IECON*, Oct. 2016, pp. 1590–1595.

[25] A. S. Abdel-Khalik, S. Ahmed, and A. M. Massoud, "Dynamic modeling of a five-phase induction machine with a combined star/pentagon stator winding connection," *IEEE Trans. Energy Convers.*, vol. 31, no. 4, pp. 1645–1656, Dec. 2016.

[26] L. Schreier, J. Bendl, and M. Chomat, "Influence of space harmonics on properties of six-phase induction machine—Part I. Analysis," in *Proc. Conf. ICEM*, Sep. 2010, pp. 1–6.

[27] L. Schreier, J. Bendl, M. Chomat, and M. Skalka, "Influence of space harmonics on properties of six-phase induction machine—Part II. Simulation and experiments," in *Proc. Conf. ICEM*, Sep. 2010, pp. 1–6.

[28] E. A. Klingshirn, "High phase order induction motors—Part I-description and theoretical considerations," *IEEE Trans. Power App. Syst.*, vol. PAS-102, no. 1, pp. 47–53, Jan. 1983.

[29] G. K. Singh, "Multi-phase induction machine drive research—A survey," *Electr. Power Syst. Res.*, vol. 61, no. 2, pp. 139–147, 2002.

[30] T. A. Lipo, "A d-q model for six phase induction machines," in *Proc. Int. Conf. Electr. Mach. (ICEM)*, 1980, pp. 860–867.

[31] X. Sun, Y. Shen, S. Wang, G. Lei, Z. Yang, and S. Han, "Core losses analysis of a novel 16/10 segmented rotor switched reluctance BSG motor for HEVs using nonlinear lumped parameter equivalent circuit model," *IEEE/ASME Trans Mechatronics*, vol. 23, no. 2, pp. 747–757, Apr. 2018.

[32] H. R. Fudeh and C. M. Ong, "Modeling and analysis of induction machines containing space harmonics part III: Three-phase cage rotor induction machines," *IEEE Trans. Power App. Syst.*, vol. PAS-102, no. 8, pp. 2621–2628, Aug. 1983.

[33] A. S. Abdel-Khalik, M. I. Masoud, S. Ahmed, and A. Massoud, "Effect of current harmonic injection on constant rotor volume multiphase induction machine stators: A comparative study," *IEEE Trans. Ind. Appl.*, vol. 48, no. 6, pp. 2002–2013, Nov./Dec. 2012.

[34] A. S. Abdel-Khalik, A. M. Massoud, and S. Ahmed, "Effect of DC-link voltage limitation on postfault steady-state performance of asymmetrical six-phase induction machines," *IEEE Trans. Ind. Electron.*, vol. 65, no. 9, pp. 6890–6900, Sep. 2018.

[35] A. S. Abdel-Khalik, A. M. Massoud, and S. Ahmed, "Nine-phase six-terminal induction machine modeling using vector space decomposition," *IEEE Trans. Ind. Electron.*, vol. 66, no. 2, pp. 988–1000, Feb. 2019.

[36] A. S. Abdel-Khalik, R. A. Hamdy, A. M. Massoud, and S. Ahmed, "Post-fault control of scalar (V/f) controlled asymmetrical six-phase induction machines," *IEEE Access*, vol. 6, pp. 59211–59220, 2018.

AYMAN S. ABDEL-KHALIK (SM'12) received the B.Sc. and M.Sc. degrees in electrical engineering from Alexandria University, Alexandria, Egypt, in 2001 and 2004, respectively, and the Ph.D. degree in electrical engineering from Alexandria University and Strathclyde University, Glasgow, U.K., in 2009, under a dual channel program. He is currently an Associate Professor with the Electrical Engineering Department, Faculty of Engineering, Alexandria University. His current research interests include electrical machine design and modeling, electric drives, energy conversion, and renewable energy. He serves as an Associate Editor for the *IET Electric Power Applications Journal* and the Executive Editor for the *Alexandria Engineering Journal*.

RAGI A. HAMDY received the B.Sc. and M.Sc. from Alexandria University, Alexandria, Egypt, in 1991 and 1994, respectively, and the Ph.D. degree from Heriot-Watt University, U.K., in 1999. He is currently an Associate Professor with the Electrical Engineering Department, Faculty of Engineering, Alexandria University. His current research interests include electric machines, electric drives, and power electronics.

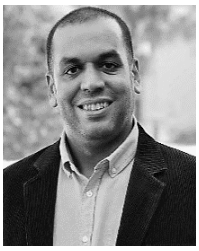

AHMED M. MASSOUD (SM'11) received the B.Sc. (hons.) and M.Sc. degrees in electrical engineering from Alexandria University, Egypt, in 1997 and 2000, respectively, and the Ph.D. degree in electrical engineering from Heriot-Watt University, Edinburgh, U.K., in 2004. He is currently an Associate Professor with the Department of Electrical Engineering, College of Engineering, Qatar University. His research interests include power electronics, energy conversion, renewable energy, and power quality. He holds five U.S. patents. He has published more than 100 journal papers in the fields of power electronics, energy conversion, and power quality.

SHEHAB AHMED (SM'12) received the B.Sc. degree in electrical engineering from Alexandria University, Alexandria, Egypt, in 1999, and the M.Sc. and Ph.D. degrees from the Department of Electrical and Computer Engineering, Texas A&M University, College Station, TX, USA, in 2000 and 2007, respectively. From 2001 to 2007, he was with Schlumberger Technology Corporation, Houston, TX, USA, where he was involved in developing the downhole mechatronic systems for oilfield service products. From 2007 to 2018, he was with Texas A&M University, Qatar (currently on leave). He is currently a Professor of electrical engineering with the CEMSE Division, King Abdullah University of Science and Technology, Saudi Arabia. His research interests include mechatronics, solid-state power conversion, and electric machines and drives.